ResearchGate

See discussions, stats, and author profiles for this publication at: https://www.researchgate.net/publication/347871210

Probabilistic multiple cracking model of brittle-matrix composite based on a one-by-one crack tracing algorithm

Article *in* Applied Mathematical Modelling · April 2021

DOI: 10.1016/j.apm.2020.10.041

CITATIONS
0

READS
26

5 authors, including:

Rostislav Chudoba
RWTH Aachen University
159 PUBLICATIONS **875** CITATIONS
SEE PROFILE

Yingxiong Li
South China University of Technology
10 PUBLICATIONS **70** CITATIONS
SEE PROFILE

Rostislav Rypl
Czech Technical University in Prague
28 PUBLICATIONS **57** CITATIONS
SEE PROFILE

Homam Spartali
RWTH Aachen University
4 PUBLICATIONS **0** CITATIONS
SEE PROFILE

Some of the authors of this publication are also working on these related projects:

Deciphering the mechanisms of mammary epithelial branched pattern formation through iterative biological and mathematical modelling View project

Optimized Designs of Experiments and sampling strategies for Monte Carlo simulations View project

All content following this page was uploaded by Yingxiong Li on 02 April 2021.

The user has requested enhancement of the downloaded file.

Applied Mathematical Modelling 92 (2021) 315–332

Contents lists available at ScienceDirect

Applied Mathematical Modelling

journal homepage: www.elsevier.com/locate/apm

Probabilistic multiple cracking model of brittle-matrix composite based on a one-by-one crack tracing algorithm

Rostislav Chudoba[a], Yingxiong Li[b,*], Rostislav Rypl[c], Homam Spartali[a], Miroslav Vořechovský[d]

[a] Institute of Structural Concrete, RWTH Aachen University, Germany
[b] School of Civil Engineering and Transportation, South China University of Technology, China
[c] AXA Insurance Company, Brno, Czech Republic
[d] Institute of Structural Mechanics, Brno University of Technology, Czech Republic

ARTICLE INFO

Article history:
Received 20 August 2020
Revised 12 October 2020
Accepted 25 October 2020
Available online 9 November 2020

Keywords:
Probabilistic modeling
Strain hardening
Matrix fragmentation
Uniaxial tensile test
Brittle-matrix composite

ABSTRACT

The paper describes a probabilistic model capturing the multiple-cracking behavior of unidirectional brittle-matrix composites loaded in tension. The approach to modeling of composite fragmentation introduces two salient features that enhance both efficiency and flexibility compared to existing simulation methods: First, the algorithm identifies the emerging cracks one by one within a minimum number of load increments. Second, the crack-tracing algorithm is based on an abstract description of a crack bridge behavior. As a result, it is possible to combine the crack-tracing algorithm with a wide variety of crack bridge models, i.e. non-linear, deterministic or probabilistic. In this way, specific phenomena of bond behavior in different types of composites can be accounted for. The random nature of matrix cracking is reproduced using a random field simulation of the matrix strength. The model is verified by reproducing analytical results available for constant bond-slip law. The feasibility and robustness of the algorithm is demonstrated using an interactive web application that is directly executable from within a public github.com repository.

© 2020 Elsevier Inc. All rights reserved.

1. Introduction

The development of multiple cracks in the matrix of brittle-matrix composites loaded in tension increases their toughness and ductility. These favorable properties endow the composite material a higher impact resistance and stress redistribution capacity [1–5]. Gradual evolution of multiple cracks along a tensile zone leads to strain-hardening behavior of the composite. A detailed description of the tensile behavior is of crucial importance for the realistic evaluation of deformation, crack width and crack spacing in the serviceability limit state [6–10]. Adjustable strain-hardening characteristics of brittle-matrix composites are desirable for many newly emerging materials, e.g. in novel fibre reinforced geopolymer (cement-free) composites [11], hybrid fiber-reinforced polypropylene [12] and cement-based composites [3,4,13].

With the enormous design space of composites opened up by the countless possible combinations of novel materials, efficient and robust characterization methods become essential. Uni-axial tensile test has been recommended as one of the

* Corresponding author.:.
E-mail address: liyingxiong@live.com (Y. Li).

https://doi.org/10.1016/j.apm.2020.10.041
0307-904X/© 2020 Elsevier Inc. All rights reserved.

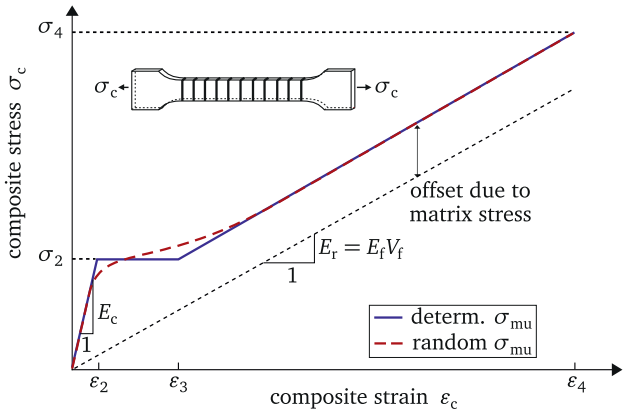

σ_{mu} matrix strength
σ_{fu} reinforcement strength

$$\varepsilon_2 = \frac{\sigma_{mu}}{E_m}, \qquad \sigma_2 = \varepsilon_2 E_c$$

$$\varepsilon_3 = \frac{\sigma_{mu}}{E_m}(1 + 0.666\alpha_e), \quad \alpha_e = \frac{E_m(1-V_f)}{E_f V_f}$$

$$\varepsilon_4 = \varepsilon_3 + \frac{\sigma_4 - \sigma_2}{E_r}, \qquad \sigma_4 = \sigma_{fu} V_f$$

Fig. 1. Stress-strain curve of a unidirectional composite under tension: deterministic matrix strength σ_{mu} (solid line) with the characteristic values specified according to Aveston-Cooper-Kelly (ACK) model; random matrix strength σ_{mu} (dashed line).

standard experimental procedures for textile-reinforced concrete [14]. Specialized models of minimal necessary complexity and dimensionality, which capture the relevant mechanisms in standardized test setups, represent a paramount prerequisite for the development of reliable, realistic and widely applicable industry standards for newly developed engineering materials. With these models, material parameters that characterize the interaction of matrix and reinforcement can be derived from 1D tensile tests and then applied in more complex numerical models of the composite material under 2D and 3D loading [1,15].

The tensile behavior of fiber reinforced composites is dependent on the properties of the matrix, the fibers, and their interface [16–18]. Typically, the stress-strain response starts with an initial linear stage as depicted in Fig. 1, the stiffness of which can be determined by the mixtures rule as

$$E_c = E_f V_f + E_m(1 - V_f) \tag{1}$$

with E_f and E_m denoting the fiber and matrix moduli of elasticity, respectively, and V_f being the fiber volume fraction. When the matrix strength is reached upon further loading, multiple cracks (matrix fragmentation) start to develop and the stiffness decreases. In the multiple cracking phase, stress redistribution occurs both between and within the constituents. This phase continues until the distance between cracks becomes shorter than the length needed to transfer a sufficient amount of stress to initiate another crack between two matrix cracks. Subsequently the composite enters the third phase featured again by a linear stress-strain response with stiffness reduced to $E_f V_f$. The vertical offset of the composite stress in the third phase from the equivalent response of pure reinforcement $E_f V_f \varepsilon_c$, with ε_c denoting the global strain, is due to the tensile stress accumulated in the matrix fragments (see Fig. 1).

Analytical solutions to the tensile response of brittle-matrix composites are only available for a few cases based on specific assumptions on constituents and their interface. In particular, several models have been developed under the assumption of a constant frictional bond in the debonded interface and a linear-elastic constitutive law for both reinforcement and matrix, with brittle failure upon reaching their strengths. The ACK model developed by Aveston, Cooper and Kelly [19] is the first model of this kind. It represents the composite tensile response by a trilinear law; see the solid line in Fig. 1. The ACK model assumes that multiple cracking occurs at a constant level of applied stress, inducing the a horizontal branch in the stress-strain behavior. The matrix fragmentation process has been thoroughly studied in [20] based on the statistical theories of the 'car parking problem' and 'crystal growth' [21,22]. For its simplicity, this model has been utilized for the simulation of tensile response of cementitious composites [23].

The aim to reproduce the experimentally observed smooth transition between the stiffness E_c of the initial phase and the stiffness $E_f V_f$ in the saturated state (see the dashed line in Fig. 1) led to the development of enhanced models accounting for the energy balance during matrix cracking and fiber debonding [24,25]. A few years later, the random matrix strength was identified as another source of the increasing stress during the multiple cracking stage [17,26,27].

According to Castelier et al. [28], the modeling approaches to multiple matrix cracking with random strength can be roughly classified into the following three categories: the random strength approach [29–32]; the random crack approach [17,33,34] and the continuous approach [27,35,36]. The listed models are analytical or semi-analytical and incorporate the randomness in both matrix and fiber strength. In the present model, we extend the random strength approach in order to account for the interaction of crack bridges that can be described by different types of crack bridge models.

An incremental fragmentation algorithm has been also utilized in the simulation of beam bending behavior. Instead of one-dimensional tensile crack bridges, elastic rotational springs have been dynamically inserted into the originally continuous model [37]. Crack initiation and coalescence of multiple cracks in a sheet of material has been simulated using a probabilistic approach in [38].

The development of the present model was motivated by the need to thoroughly characterize the tensile behavior of various types of brittle-matrix composites. In particular, it has been driven by the need to describe the behavior of textile-reinforced concrete (TRC), a cementitious composite with heterogeneous material structure of matrix, reinforcement and bond at overlapping scales of resolution. Even though the original goal was to model the tensile response of TRC, the resulting modeling framework is general and can be applied to various types of composites exhibiting fragmentation upon tensile loading. In the present paper, a generic algorithm is proposed for the multiple cracking process that can be conveniently combined with a variety of crack bridge models to simulate different types of composites, e.g.

- analytical crack bridge models with constant frictional bond in the interface [23,39];
- finite-element crack bridge models with nonlinear material laws for reinforcement and bond [40];
- micromechanical probabilistic crack bridge models reflecting random material properties of the reinforcement and bond [39,41].

Besides the modeling approach to multiple cracking and debonding, the paper presents the model implementation exploiting the modern concepts of scientific computing provided within the `Python` package ecosystem, including the `NumPy` and `SciPy` packages. Similar aims have been recently applied for the simulation of fragmentation of a continuum [42]. Unlike in [43] where `Python` was used as a scripting language and front-end to control a finite element solver implemented in `C` language, the present implementation approach exploits the features and data model provided in `NumPy`. Based on the vectorized evaluation of the mathematical expression using high-level compiled functions available in the compiled packages, it is possible to develop highly efficient software with a code that closely follows the original structure and expressiveness of the mathematical model description.

The recently emerging support for developing scientific application with the `Python` package ecosystem has been bundled within the `Jupyter` framework. In comparison with the high-level tools, like `Mathematica`, `Maple`, or `Matlab`, `Jupyter` enables a seamless transition between the prototyping phase of a mathematical model to scientific publications and courses interleaved with executable model examples. Moreover, models can be easily transformed to full-fledged interactive web applications, accessible via any browser and executable on a remote computer. This feature is demonstrated at the end of the paper with a sample implementation of the multiple-cracking model.

The remainder of the paper is organized as follows: Section 2 describes the probabilistic multiple cracking model (PMCM) at the macroscale. The link to the crack bridge models is presented in Section 3. Section 4 discusses the salient features of the model in detail. The model is then verified based on available analytical solutions in Section 5. An example of the model application is presented in Section 6 using tensile tests published in the literature [23]. Finally, conclusions are drawn in Section 7.

2. Probabilistic multiple cracking model

2.1. Random strength approach

Probabilistic modeling approaches for composites with brittle fragmentation in one of its constituents can be found in several papers, e.g. [8–10,24,27]. In the case of a brittle matrix, it can be assumed that cracks immediately run through the entire cross-section after initiation. This behavior reveals an unstable crack propagation. Therefore an energetic treatment of the crack propagation is not necessary and the strength criterion captures the stress level during crack initiation and its full development sufficiently well. The class of methods generally referred to as “random strength approach” [28] can be qualitatively explained with the sketched matrix stress states at several selected load levels in Fig. 2.

To reflect the randomness in matrix strength along the specimen, the matrix strength profile shown by the red wavy line in Fig. 2a–d was generated by a single realization of a random field. Under tension, the first crack appears at the minimum point of matrix strength profile and the corresponding matrix stress profile along the specimen is shown in Fig. 2a. Then, the matrix stress increases upon further loading until the matrix strength is reached at other locations (Fig. 2b, c). Each time the matrix strength is reached, a new crack is added into the numerical representation of the specimen. Then the stress profile is updated according to the considered material properties. At a cracked position, the matrix stress drops to zero and a certain length along the reinforcement is required to reach the level of the matrix strength. The segment of matrix within this stress transfer length is in a sense shielded by the existing crack. Thus, after reaching a certain crack density the whole specimen shall be covered by the shielded zones and no more cracks can appear (Fig. 2d). At this point, the saturated state of cracking has been attained.

In a specimen with multiple parallel cracks, each segment near a crack is subjected to similar boundary conditions so that it can be modeled using a representative crack bridge model. Utilizing this periodicity the computational demand and complexity can be drastically reduced. As a consequence, a crack bridge model accounting for local damage processes within the microstructure of the composite can be employed. The crack bridge model is required to deliver the matrix stress profile σ_{m} and the crack width w as functions of the applied remote stress σ_{c}. A simple example of these crack bridge functions for the basic case of a constant frictional bond model is provided in Fig. 3. This crack bridge model will be explained in a more detail later on in Section 3 and will be used in the verification studies in Section 5.

For a given composite stress level, the nominal composite strain can be determined by averaging the strain profiles of the reinforcement. The process of crack detection, stress profile update and nominal strain evaluation is iterated until the

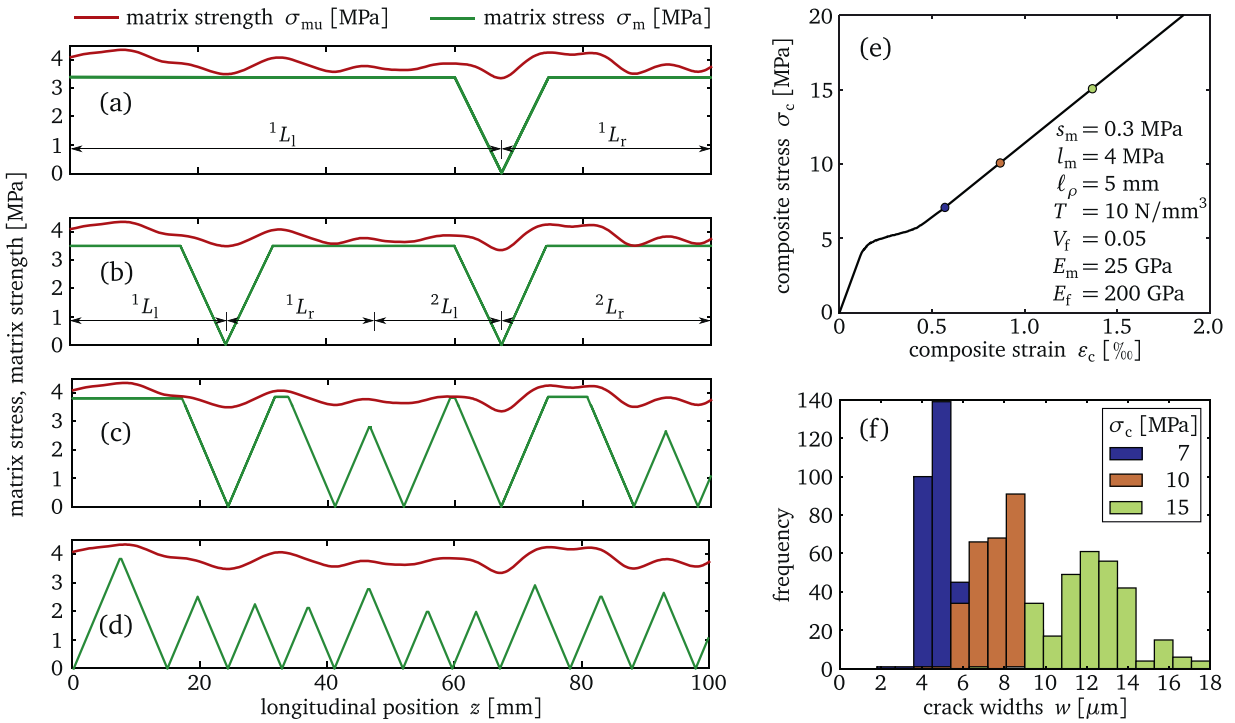

Fig. 2. Graphical representation of the random matrix strength approach: (a) – (d) development of matrix cracks in a composite specimen; (e) stress-strain relationship; (f) histograms of crack width at different load levels.

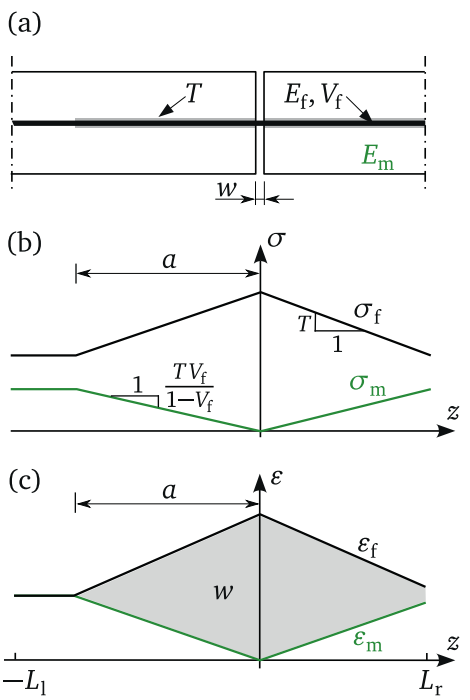

E_m matrix modulus
E_f reinforcement modulus
E_c composite modulus given by Eq. (1)
T bond intensity
V_f reinforcement volume fraction
σ_c remote stress
w crack opening

$$\sigma_m = \begin{cases} \dfrac{TV_f}{1-V_f}|z| : & |z| < a \\ \dfrac{\sigma_c E_m}{E_c} : & |z| \geq a \end{cases}$$

$$a = \frac{\sigma_c E_m (1-V_f)}{E_c T V_f}$$

$$\varepsilon_f = \frac{\sigma_c - (1-V_f)\sigma_m}{E_f V_f}$$

$$\varepsilon_m = \sigma_m / E_m$$

$$w = \int_{-L_l}^{L_r} (\varepsilon_f - \varepsilon_m)\, dz$$

Fig. 3. Analytical solution of a crack bridge with constant bond: (a) the crack bridge model; (b) the reinforcement stress σ_f and matrix stress σ_m; (c) the reinforcement stain ε_f and matrix strain ε_m.

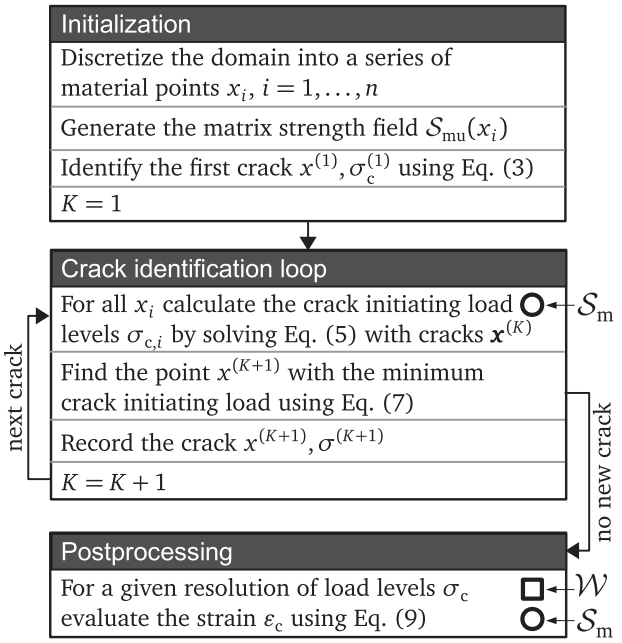

Fig. 4. Schematic of the crack tracing algorithm.

saturated state has been achieved. The algorithm delivers the composite stress-strain relationship as shown in Fig. 2e. In the meantime, the widths of all matrix cracks can be readily determined for any level of applied composite stress; see Fig. 2f. This detailed output facilitates the sensitivity analysis of the tensile behavior with respect to the input parameters and their statistical variability. The material parameters used in the present example are listed in Fig. 2e. The statistics of the crack widths were obtained with the model of a 3000 mm long composite specimen. For brevity, the matrix strength and stress profiles of a 100 mm long representative segment are shown in Fig. 2(a-d).

2.2. General crack tracing algorithm

Detailed mathematical description as a guide for its generic implementation is exlplained based on the flowchart shown in Fig. 4 for a discretized tensile specimen length, L_{c} (the length measured along the loading direction). For mathematical rigour, the individual steps of the algorithm are described based on a continuous representation of a composite specimen covering the domain $x \in [0, L_{\mathrm{c}}]$.

I. Initialization The matrix tensile strength, σ_{mu}, is generated by sampling a prescribed random field. It is represented by a function of the global coordinate x

$$\sigma_{\mathrm{mu}} = \mathcal{S}_{\mathrm{mu}}(x). \tag{2}$$

Let the cracks be enumerated by an index K. In the initial state $K = 0$ without any cracks, the matrix stress is constant over the whole specimen and can be evaluated explicitly according to the rule of mixtures. Then, the state of $K = 1$ is reached with the first crack emerging at the minimum point of $\mathcal{S}_{\mathrm{mu}}(x)$. Its location $x^{(1)}$ and the corresponding cracking stress level $\sigma_{\mathrm{c}}^{(1)}$ are identified as

$$x^{(1)} = \arg\min_{x \in (0, L_{\mathrm{c}})} \mathcal{S}_{\mathrm{mu}}(x), \quad \sigma_{\mathrm{c}}^{(1)} = \frac{E_{\mathrm{c}}}{E_{\mathrm{m}}} \mathcal{S}_{\mathrm{mu}}(x^{(1)}). \tag{3}$$

II. Crack identification loop Now the task is to identify the tensile load levels initiating the subsequent cracks. Let the composite stress σ_{c}, which is defined as the tensile force divided by the cross-sectional area and is thus constant over the whole specimen, serve as the control variable. Its value at the initiation of the K^{th} crack is denoted by $\sigma_{\mathrm{c}}^{(K)}$. Given a set of K existing cracks at the positions $\boldsymbol{x}^{(K)} = \{x^{(k)}\}$, $k = 1, 2, \ldots, K$ (see Fig. 5), we want to find the load level $\sigma_{\mathrm{c}}^{(K+1)} > \sigma_{\mathrm{c}}^{(K)}$ initiating the next crack and the corresponding position $x^{(K+1)}$.

To find the next location where the matrix stress reaches its strength, we first need to evaluate the stress profile at the state with K existing cracks represented by $\boldsymbol{x}^{(K)}$. To allow for a nonlinear kind of bond behavior and crack bridge representation, we assume the matrix stress at a point x is a generally *nonlinear* function of the load σ_{c} and can be expressed as

$$\sigma_{\mathrm{m}}^{(K)} = \mathcal{S}_{\mathrm{m}}(\sigma_{\mathrm{c}}, x, \boldsymbol{x}^{(K)}, \boldsymbol{\Theta}_{\mathrm{CB}}), \tag{4}$$

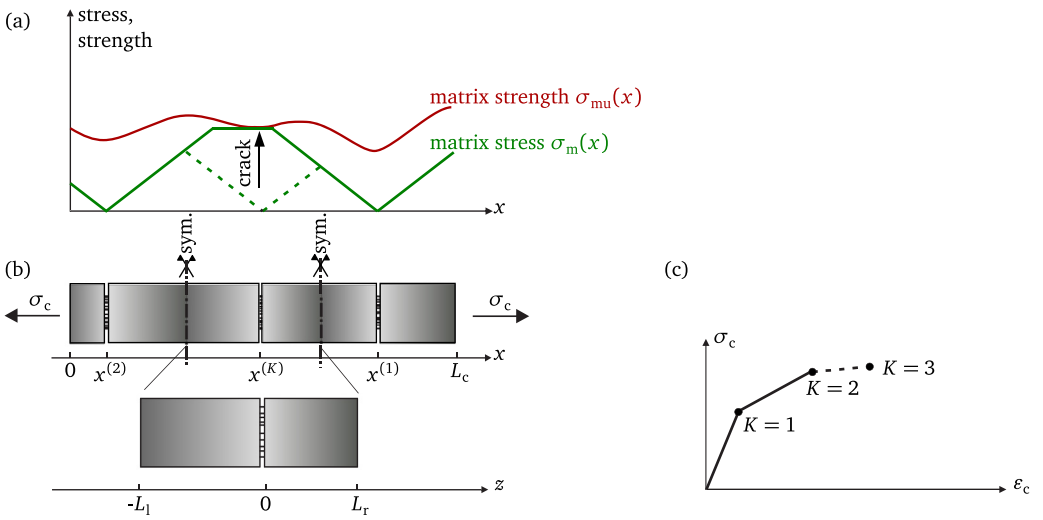

Fig. 5. The state at the initiation of the K^{th} crack: (a) stress and strength of the matrix; (b) composite specimen with a detailed representation of the K^{th} crack bridge; (c) stress-strain curve.

where $\boldsymbol{\Theta}_{\text{CB}}$ is a vector summarizing the parameters needed by the particular crack bridge model to quantify the interaction between reinforcement and matrix. Then, the level of applied remote stress σ_c that would initiate a new crack at any $x \in [0, L_c]$ must meet the following criterion: the matrix stress $\sigma_m^{(K)}$ introduced by σ_c equals the matrix strength, i.e.,

$$\mathcal{S}_m(\sigma_c, x, \boldsymbol{x}^{(K)}, \boldsymbol{\Theta}_{\text{CB}}) = \mathcal{S}_{mu}(x). \tag{5}$$

By solving this nonlinear equation at all points $x \in [0, L_c]$ we obtain the field of crack initiating loads as a function of x:

$$\mathcal{S}_c(x) := \left\{ \sigma_c \mid \mathcal{S}_m(\sigma_c, x, \boldsymbol{x}^{(K)}, \boldsymbol{\Theta}_{\text{CB}}) = \mathcal{S}_{mu}(x) \right\}. \tag{6}$$

It is noteworthy that for some x no solution can be found for Eq. (5), which indicates that those material points are located within the shielded zone of already existing cracks. Since in each step only one crack is allowed to appear, the sought load $\sigma_c^{(K+1)}$ initiating at the position x_{K+1} is obtained by finding the minimum of $\mathcal{S}_c(x)$ over $x \in [0, L_c]$:

$$x^{(K+1)} = \underset{x \in (0, L_c)}{\operatorname{argmin}} \mathcal{S}_c(x), \quad \sigma_c^{(K+1)} = \mathcal{S}_c(x^{(K+1)}). \tag{7}$$

The cracking history along with the associated state variables is obtained by running a loop over Eqs. (4) – (7) with a crack counter $K = K + 1$ (see Fig. 4). The algorithm ends if no solution to Eq. (5) can be found for any $x \in [0, L_c]$ indicating that the saturated state with K_{sat} cracks has been reached.

The final point of the stress-strain curve, which corresponds to the strength of the composite specimen, is given by the failure of the reinforcement in a crack bridge. In case of heterogeneous, distributed reinforcement, like short fibers or finely structured textile fabrics, the instantaneous crack bridge strength represents a complex question including several interacting variables, e.g. the type of bond-slip law, the type of random variables and the distances between crack bridges. By combining the PMCM with a probabilistic crack bridge model (PCBM, see e.g. [39,41]), these interactions can be taken into account as well.

III. Postprocessing The identified history of the matrix cracking states $K = 1, 2, \ldots, K_{\text{sat}}$ is adopted to evaluated the nominal stress-strain curve of the composite. Two possibilities have been included in the implementation.

In case of homogeneous reinforcement with the profile of reinforcement strain ε_f provided by the crack bridge model in analytical form, the composite strain is directly evaluated as the average reinforcement strain along the specimen length at each stage of cracking $\boldsymbol{x}^{(K)}$

$$\varepsilon_c^{(K)} = \frac{1}{L_c} \int_0^{L_c} \varepsilon_f(\sigma_c; x, \boldsymbol{x}^{(K)}, \boldsymbol{\Theta}_{\text{CB}})\, \mathrm{d}x. \tag{8}$$

In case of a multi-scale model with fine resolution of the heterogeneous reinforcement structure like short fibers [44] or multi-filament yarns considered in [39,41] it is more convenient to calculate the composite strain as a sum of the crack openings and matrix elongation divided by the specimen length. To achieve this in a generic manner, for a given crack $x^{(k)}$, $k \in 1 \ldots K$, the opening needs to be expressed as a function of the remote load σ_c within the range $\sigma_c^{(K)} \le \sigma_c < \sigma_c^{(K+1)}$:

$$w^{(k,K)} = \mathcal{W}(\sigma_c; x^{(k)}, \boldsymbol{x}^{(K)}, \boldsymbol{\Theta}_{\text{CB}}). \tag{9}$$

The particular form of $\mathcal{W}$ is supplied by the crack bridge model describing the debonding in the interface, which will be explained in detail in Section 3. With both $\mathcal{W}$ and $\mathcal{S}_\mathrm{m}$ at hand, the composite strains ε_c corresponding to the load σ_c within the range $\sigma_\mathrm{c}^{(K)} \le \sigma_\mathrm{c} < \sigma_\mathrm{c}^{(K+1)}$ can be evaluated as

$$\varepsilon_\mathrm{c}^{(K)} = \frac{1}{L_\mathrm{c}}\left[\sum_{k=1}^{K} \mathcal{W}(\sigma_\mathrm{c}; x^{(k)}, \boldsymbol{x}^{(K)}, \boldsymbol{\Theta}_\mathrm{CB}) + \frac{1}{E_\mathrm{m}} \int_0^{L_\mathrm{c}} \mathcal{S}_\mathrm{m}(\sigma_\mathrm{c}; x, \boldsymbol{x}^{(K)}, \boldsymbol{\Theta}_\mathrm{CB})\, \mathrm{d}x\right]. \tag{10}$$

The resulting stress-strain diagram (see e.g. Fig. 2e) is then evaluated piecewisely according to

$$\tilde{\mathcal{S}}_\mathrm{c}(\varepsilon) := \{\sigma^{(k)} + \frac{\sigma^{(k+1)} - \sigma^{(k)}}{\varepsilon^{(k+1)} - \varepsilon^{(k)}}(\varepsilon - \varepsilon^{(k)}), \varepsilon^{(k)} \le \varepsilon < \varepsilon^{(k+1)}\}. \tag{11}$$

Remark 1. Load control versus displacement control. In tensile test setups, displacement control is usually used to introduce the load. As a result, the measured force drops upon each crack initiation and a serrated profile is obtained in the cracking stage. The described crack tracing algorithm uses load control with a monotonically increasing composite stress so that the stress drops cannot be directly evaluated.

3. Incorporation of the crack bridge models

The above-described algorithm abstracts from the details of the debonding process in the interface such that its implementation is independent of the particular type of crack bridge model. The crack bridge model compatible with the proposed PMCM must provide two interface functions $\mathcal{S}_\mathrm{m}$ and $\mathcal{W}$ in Fig. 4, the former computing the matrix stress and the latter returning the crack width for a prescribed level of remote load σ_c. By implementing specialized crack bridge models, the proposed PMCM can be easily adapted to describe a wide range of cementitious composites, including short-fiber composites (engineered cementitious composites), composites with continuous, macroscopically homogeneous reinforcement (steel, GFRP, CFRP) bars, as well as reinforcement with multi-filament yarns (e.g. TRC) that require statistical description of the yarn and bond structure.

3.1. Elementary crack bridge model with constant friction

To verify the basic behavior of the proposed crack tracing algorithm, we formulate a simple crack bridge model considering constant frictional stress transmitted by the interface as illustrated in Fig. 3. For convenience the crack bridge model is formulated based on the local coordinate z (in contrast to the global coordinate x used in the crack tracing algorithm of PMCM) which is equal to zero at the crack position. The local state function $\tilde{\mathcal{S}}_\mathrm{m}$ required for evaluating the matrix stress can be explicitly obtained as

$$\sigma_\mathrm{m} = \begin{cases} \dfrac{TV_\mathrm{f}}{1-V_\mathrm{f}}|z| & : |z| < a \\ \dfrac{\sigma_\mathrm{c}E_\mathrm{m}}{E_\mathrm{c}} & : |z| \ge a \end{cases} \tag{12}$$

where $T = 2\tau/r$ is defined as the bond intensity with τ being the magnitude of bond and r being the reinforcement radius, and E_c is the composite stiffness defined in Eq. (1). The instantaneous debonded length a (see Fig. 3b) is defined as the position z at which the linearly increasing matrix stress reaches the level of the applied remote stress (equality of the two branches in Eq. (12)):

$$a = \frac{\sigma_\mathrm{c}E_\mathrm{m}(1-V_\mathrm{f})}{E_\mathrm{c}TV_\mathrm{f}}. \tag{13}$$

The resulting matrix strain profile $\varepsilon_\mathrm{m} = \sigma_\mathrm{m}/E_\mathrm{m}$ and the corresponding reinforcement strain profile

$$\varepsilon_\mathrm{f} = (\sigma_\mathrm{c} - \sigma_\mathrm{m})/E_\mathrm{f} \tag{14}$$

near the crack are shown in Fig. 3(b). The other required function, crack opening $\mathcal{W}$, can be easily calculated as the gray area in Fig. 3(c).

3.2. Mapping between global and local domains

To introduce an abstraction barrier between PMCM and the crack bridge model, we have to define the mapping between the global coordinate x of the tensile specimen and the local coordinate z centered at individual crack bridges. The defined mapping reflects the symmetry of stress profiles about the midpoint between adjacent cracks (see Fig. 5b) in a multiply cracked composite. The domain of a crack bridge is then given as $z \in [-L_\mathrm{l}, L_\mathrm{r}]$, with L_l and L_r being the distances from the

midpoint to the nearest left and right cracks, respectively. At these midpoints, the reinforcement displacement equals the displacement of the matrix such that there is no slip in the bond interface.

To provide a flexible mapping between $x \in [0, L_c]$ and $z \in [-L_l, L_r]$, we introduce an index function to find the crack $\kappa \in \{1, 2, \ldots, K\}$ having the shortest distance to a given x

$$\kappa(x) = \underset{x^{(k)} \in \boldsymbol{x}^{(K)}}{\operatorname{argmin}} |x - x^{(k)}|. \tag{15}$$

Since the local coordinate z can be viewed as the signed distance from a point to its nearest crack, a function mapping x to z can be written as

$$z(x) = x - x^{(\kappa(x))}, \tag{16}$$

where $x^{(\kappa(x))}$ denotes the global coordinate of the nearest crack. Negative z indicates the material point x on the left side from its nearest crack and positive z on its right side. The values L_l and L_r, delimiting the domain of a crack bridge instance that a material point x belongs to, can be evaluated in a similar manner:

$$\begin{aligned} L_l(x) &= \min(x^{(\kappa(x))} - x^{(k)}), \ \forall x^{(k)} \in \boldsymbol{x}^{(K)} \cap [0, x^{(\kappa(x))}); \\ L_r(x) &= \min(x^{(k)} - x^{(\kappa(x))}), \ \forall x^{(k)} \in \boldsymbol{x}^{(K)} \cap (x^{(\kappa(x))}, L_c]. \end{aligned} \tag{17}$$

To avoid duplicate solutions of the incorporated crack bridge model for symmetric pairs (L_l, L_r) and (L_r, L_l), for each crack bridge its boundaries are rearranged to distinguish the shorter and longer side as (see Fig. 5)

$$\begin{aligned} L_\downarrow(x) &= \min(L_l(x), L_r(x)); \\ L_\uparrow(x) &= \max(L_l(x), L_r(x)). \end{aligned} \tag{18}$$

Based on these mappings, the interface between the PMCM and the crack bridge model can be narrowed down to the following locally defined crack bridge functions:

$$\sigma_m = \tilde{\mathcal{S}}_m(\sigma_c; z, L_\downarrow, L_\uparrow, \boldsymbol{\Theta}_{CB}), \tag{19}$$

representing the matrix stress profile, and

$$w = \tilde{\mathcal{W}}(\sigma_c; L_\downarrow, L_\uparrow, \boldsymbol{\Theta}_{CB}). \tag{20}$$

evaluating the crack opening. These crack-centered functions are instantiated for each new crack identified by the PMCM on the fly by supplying the mapping fields $z(x)$ and $L_\downarrow(x), L_\uparrow(x)$ given in Eqs. (16) and (18) into Eqs (19) and (20). Then, the required stress and strain profiles required in Eqs. (5) and (10) are efficiently evaluated from a single, crack-centered crack bridge model.

The crack tracking algorithm described in Section 2.2, the simple crack bridge model presented in Section 3.1 and the mapping technique constitute a minimal working configuration of the proposed modeling framework. All the three components can be efficiently implemented using the `Python` based open source tools such as the `NumPy` library for vectorized manipulation of n-dimensional arrays [45]. The implementation of the framework along with the obtained executable `Python` code is explained in Appendix A and provided as an interactive web application [46].

Let us remark, that the mapping introduced between the local state in the vicinity of a crack bridge and the global state of a tensile specimen represents a novel feature of crack-tracing algorithms. Indeed, the distinct crack-centered coordinate z and the global position x can be used to separate the scales of resolution of strains and stresses at the local and global levels. The algorithm is able to incorporate the crack bridge instances with detailed crack-bridge resolution at newly initiated cracks *on-the-fly*. This feature has been already exploited by the authors using a probabilistic model of a crack bridge in combination with the presented adaptive crack-tracing approach to simulate the strain-hardening response of TRC composite reinforced with non-penetrated multi-filament yarns [39].

3.3. Numerical inversion of crack bridge models

The example of a crack bridge model shown in Section 3.1 represents a special case with analytically derived state functions. In general, however, it is not possible to express the matrix stress σ_m and the crack opening w as explicit functions of the composite stress σ_c. Available crack bridge models from the literature [39,41,44,47,48] usual provide an inverse mapping, i.e. the crack bridging force F as a function of the crack opening w, the bridge lengths $L_\downarrow, L_\uparrow$ and other relevant parameters summarized in the vector $\boldsymbol{\Theta}_{CB}$. Using these models the composite stress at the crack can be obtained as

$$\sigma_c = \frac{F(w; L_\downarrow, L_\uparrow, \boldsymbol{\Theta}_{CB})}{A_c}, \tag{21}$$

where A_c is the area of the composite section.

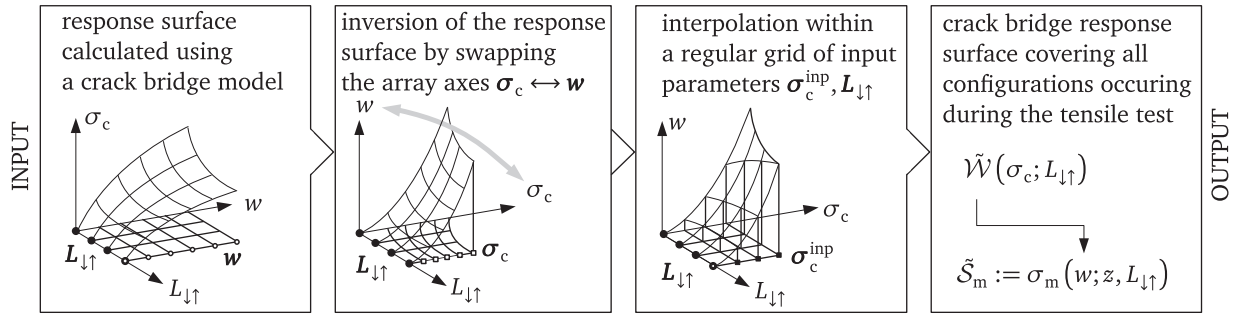

Fig. 6. A compatible crack bridge response surface obtained with numerical inversion and interpolation.

To use these models in combination with the PMCM controlled by the applied composite stress σ_c we need to invert the bridging function $\sigma_c(w; L_\downarrow, L_\uparrow, \boldsymbol{\Theta}_{CB})$ in Eq. (21) into the form of Eq. (20). Since a general analytical inversion is not possible a numerical inversion has been implemented as sketched in Fig. 6. First, the crack bridge response up to the maximum bridging force is evaluated for each pair of crack bridge lengths $\boldsymbol{L}_{\downarrow\uparrow}$ that might be encountered during the fragmentation process. Second, the inversion of the response surface is performed by swapping the array axes $\boldsymbol{\sigma}_c$ and $\boldsymbol{w}$. Finally, the response surface for crack opening w is transformed to a regular interpolation grid $\boldsymbol{\sigma}_c^{inp} \times \boldsymbol{L}_{\downarrow\uparrow}$ of the input parameters to obtain the numerical approximation of Eq. (20). In this way, it is prepared as a plug-in into the open slot $\mathcal{W}$ of the PMCM shown in Fig. 4.

The second required response surface, $\mathcal{S}_m$ delivering the matrix stress profile near the crack is constructed by performing a numerical substitution. In particular, the crack bridge models controlled by the crack opening provide the matrix stress profile as a function $\sigma_m(w; z, L_\downarrow, L_\uparrow, \boldsymbol{\Theta}_{CB})$, in which z is the local coordinate (Fig. 3), see e.g. [39]. The plug-in delivering the stress profile $\mathcal{S}_m$ is constructed by substituting the inverted $\mathcal{W}$ response surface into σ_m as indicated in the last step of Fig. 6.

The numerical inversion technique is applicable to many types of crack bridge models. In [49] it has been used in combination with a deterministic, finite element crack bridge model with generally non-linear bond-slip law, with which the tensile behavior of TRC reinforced by styrene-butadiene penetrated textile fabrics was studied. In [39], we used it with the probabilistic crack bridge model [50] to simulate TRC with non-impregnated carbon yarns exhibiting a high degree of heterogeneity.

4. Salient features of the crack tracing algorithm

Compared to existing models, the proposed PMCM introduces two important extensions. It is robust with respect to algorithmic parameters and it accepts nonlinear bond-slip laws with softening.

4.1. Adaptive load control

In the crack tracing models based on the "random strength approach" [8,28,44,51], small constant load increments are used to control the computation. In each load step, the matrix cracking criterion is checked to decide whether or not the matrix stress exceeds the strength. As a result, in a single increment several material points along the specimen may exceed the matrix strength. If these material points are far enough from each other to avoid interaction through their adjacent debonding zones, simultaneous insertion of several cracks in one load increment is possible. However, if interaction cannot be excluded a decision must be made how to treat the simultaneous appearance of several cracks. In such a case, the order of appearance of interacting cracks is important. A possible solution is to reduce the load increment such that only one crack would appear. However, if the scatter of the matrix strength is very small, this approach is not robust with respect to the algorithmic parameters and, moreover, becomes computationally demanding. In contrast, the procedure described in Section 2 calculates the load increment such that only one crack can appear in a single load step. This feature is preserved for any kind of bond-slip law defining the crack bridge behavior.

4.2. Nonlinear crack bridge response

To demonstrate the ability of the model to handle a general type of bond behavior, let us compare the development of matrix stress in the vicinity of a crack for the cases of *constant* and *nonlinear* bond-slip laws shown in Figs. 7a and b, respectively. Consider an imaginary tensile specimen with one crack bridge that exhibits constant bond-slip law at the left side and non-linear bond-slip law with softening at the right side of the crack as indicated in Fig 7 c. The matrix stress profiles corresponding to a series of applied composite stress levels $1, 2, \ldots, 12$ MPa are sketched below. We remark that all

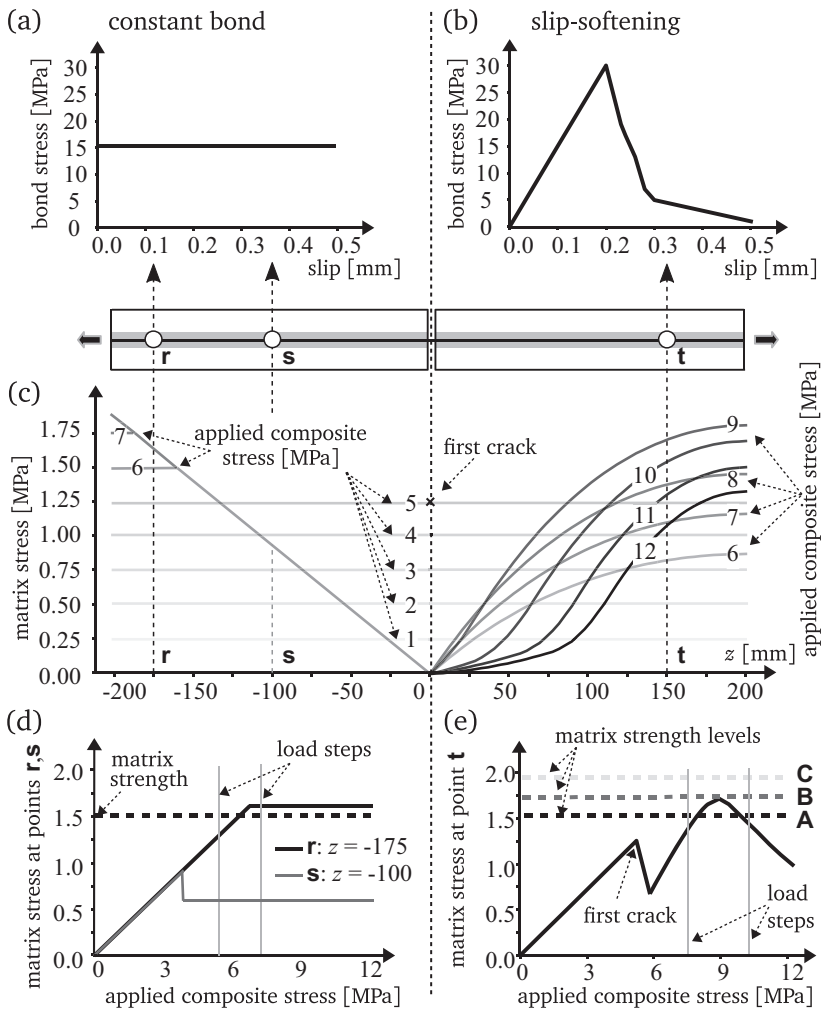

Fig. 7. Comparison of local matrix stress development for two types of bond-slip laws: (a) constant bond-slip law; (b) bond-slip law with softening; (c) matrix stress profiles for increasing loading levels, each stress profile is marked by the corresponding applied stress level; (d) matrix stress development for constant bond stress law at points **r**: $z = -175$ mm and **s**: $z = -100$ mm; (e) matrix stress development for slip-softening law at point **t**: $z = 150$ mm.

the profiles of matrix stresses in Fig. 7 are quantitatively evaluated using an efficient finite element model of a crack bridge implemented using open source scientific computing Python package numpy [18].

Let us assume that the first crack has emerged at the applied composite stress of $\sigma_c = 5$ MPa at the position $z = 0$ mm. Up to this load level, the matrix stress was constant along the whole specimen as depicted by the horizontal lines for the composite stress levels $\sigma_c = 1, 2, \ldots, 5$ MPa in Fig. 7(c). During this phase, the matrix stress has been increasing linearly in the whole domain of the specimen. After the appearance of the first crack, the matrix stress dropped to zero at the crack position $z = 0$ and debonding started in its vicinity. Within the debonded zone, the stress transfer from the reinforcement to the matrix was governed by the bond-slip law.

Considering the constant bond-slip law shown in Fig. 7(a) and follow the stress development at two selected material points **r**: $z = -175$ mm and **s**: $z = -100$ mm. The relationships between matrix stress and applied load at these two points are shown in Fig. 7(d). Assuming that the matrix strength at the considered points is $\sigma_{mu} = 1.5$ MPa (thick dashed line), we see that the matrix stress at the point **r** approaches the strength linearly and will achieve this value before **r** being reached by the shielded zone develops from the crack. On the other hand, the point **s** will exhibit a drop in the matrix stress upon the initiation of the first crack shown as the gray line in Fig. 7(d). From that moment on, the matrix stress at **s** stays constant and no crack can be initiated there. In this sense, **s** is shielded by the crack.

In case of a nonlinear bond-slip law with a descending branch shown in Fig. 7(b), the matrix stress profiles at the right hand side of the crack (Fig. 7c) have been calculated using a finite element crack bridge model [49] and numerically inverted to associate them with the levels of applied composite stress σ_c (see Fig. 6). Regarding a material point **t**: $z = 150$ mm and

following its matrix stress evolution for the increasing level of composite stress in Fig. 7(e) we observe a drop of the matrix stress at the appearance of the first crack and its subsequent growth in correspondence to the nonlinear bond slip law up to the point when the maximum level of bond stress has been reached. The intersection of the curve describing the matrix stress evolution (solid line) with the level of the local matrix strength (dashed line) represents the cracking level of the next crack at the point **t**. This intersection is sought using a non-linear root-finding algorithm, i.e. the Newton method.

Fig. 7 (e) considers three possible levels (**A**,**B**,**C**) of matrix strength at **t**. Given a load increment of the composite stress indicated on the horizontal axis, the intersections between the strength levels **A** or **B** with the matrix stress evolution curve exist, and will be identified by the root finding algorithm within a few iterations. In case of the strength level **C**, the material point enters the bond-slip softening regime before reaching the matrix strength and no intersection exists. This case indicates that the material point is within the shielded zone of the crack. All the three configurations are correctly handled by the proposed PMCM algorithm.

However, if discrete load increments were explicitly prescribed as in the existing models, the algorithm could not handle the considered cases in a robust way. Since the matrix cracking criterion is checked only for the load steps indicated by the vertical lines in Fig. 7(e), the crack at the point **t** would be overlooked for matrix strength levels levels **A** and **B**.

To conclude, the algorithms employing prescribed constant load steps, even with refined increments, is only able to handle the non-softening laws as shown in Fig. 7(a). The proposed PMCM can treat the complex material laws including softening behavior correctly in a more robust manner.

5. Verification

Let us document the validity of PMCM by testing its behavior in two elementary configurations. First, we consider the limiting case of a constant matrix strength and frictional bond law, analytically covered by the ACK model. In the second step, we study the effect of increasing scatter of random matrix strength on the final crack spacing and compare the obtained response with the analytical results presented by Curtin [52]. The reader can easily reproduce these two studies using the interactive online web application [46] with the material parameters adjusted according to the cases described below.

5.1. Constant matrix strength and constant bond

The first study applies the PMCM algorithm to a reinforced tensile specimen with assumed constant matrix strength and constant frictional bond. The stress-strain response for such a composite can be evaluated analytically using the ACK model. The stress-strain diagram is characterized by the points defined by $\sigma_2, \varepsilon_2, \varepsilon_3, \sigma_4$ and ε_4 shown in Fig. 1. It has three branches, the first one describes the initial uncracked stage. As mentioned before, the stiffness E_c can be evaluated using the mixture rule in Eq. (1). The starting point of the second phase$(\varepsilon_2, \sigma_2)$, which indicates the matrix strength reaches the strength σ_{mu}, can be calculated as follows

$$\varepsilon_2 = \frac{\sigma_{mu}}{E_m}, \quad \sigma_2 = \frac{\sigma_{mu}}{E_m} E_c. \tag{22}$$

Since we assume a constant matrix strength, all the cracks appear at the same stress level, thus the second branch in ACK model is horizontal. The strain ε_3 marking the end of the fragmentation process is obtained as

$$\varepsilon_3 = \left(1 + 0.666 \frac{E_m(1 - V_f)}{E_f V_f}\right) \frac{\sigma_{mu}}{E_m}. \tag{23}$$

In the third branch the applied load is only carried by the reinforcement. Thus, the stiffness of this branch reads

$$E_r = E_f V_f. \tag{24}$$

The failure of the tensile specimen occurs when the reinforcement strength is reached so that the last point in the stress-strain curve is given as

$$\begin{aligned} \sigma_4 &= \sigma_{fu} V_f, \\ \varepsilon_4 &= \varepsilon_3 + \frac{\sigma_4 - \sigma_2}{E_r} \end{aligned} \tag{25}$$

with σ_{fu} being the reinforcement strength.

To show that PMCM can reproduce the analytical results given the assumptions of the ACK model, we adopt the material parameters used in [53] that were used to roughly reproduce the tensile tests performed there. It is emphasized that our goal is not to reproduce the tests themselves, as we do not have sufficient data, but rather the ACK curves showing the stress-strain relationships for three considered reinforcement ratios.

The adopted material parameters are summarized in Table 1. The stress-strain curves obtained using PMCM and ACK models for the considered reinforcement ratios are shown in Fig. 8(a). In PMCM, the matrix strength was generated with a

Table 1
Parameters adopted from [53] .

parameter	notation	value	unit
reinforcement ratio	V_f	$0.7-1.4$	%
reinforcement modulus	E_f	67	GPa
matrix modulus	E_m	8.25	GPa
matrix strength	σ_{mu}	2.48	MPa

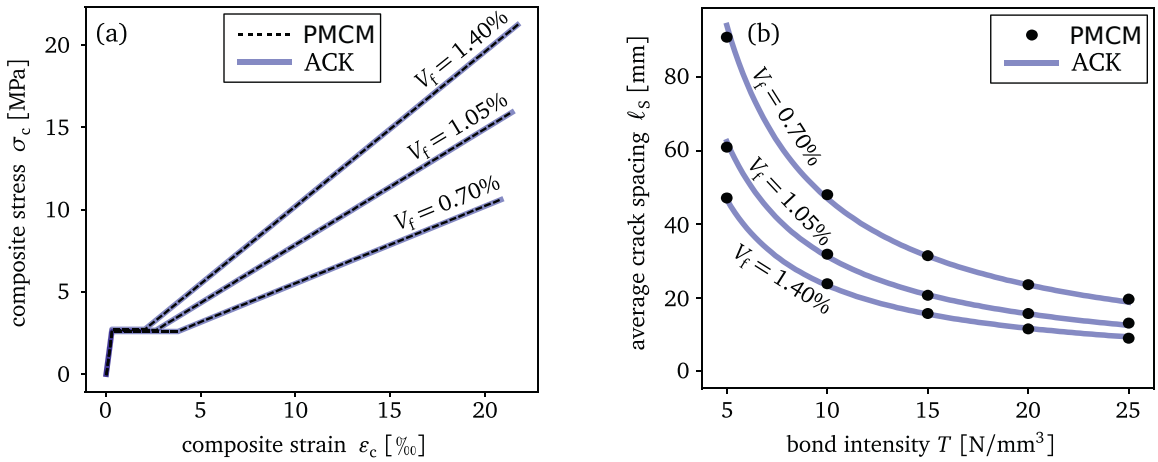

Fig. 8. Results given by PMCM and the ACK model for different reinforcement ratios: (a) stress-strain relationship; (b) final crack spacing as a function of T.

very small coefficient of variance 0.01% to mimic the constant matrix strength. The length of the simulated specimen was 5000 mm to get representative results on crack spacing.

Let us remark, that in ACK model the stress-strain relationship does not depend on the bond intensity as documented by the Eqns. 22–(25). On the other hand, for the PMCM simulation using the crack bridge model with the matrix stress profile given in Eq. (12) the bond intensity had to be specified, even though it has no effect on the stress-strain response.

The effect of the bond intensity can be studied using both models in terms of the crack spacing at the saturated state. In ACK model, the effect of bond intensity T on the final average crack spacing ℓ_{CS} is given as [22]

$$\ell_{CS} = 1.337 \frac{V_m \sigma_{mu}}{V_f T}. \tag{26}$$

In Fig. 8(b), the final crack spacings given by the PMCM are compared to the Eq. (26) for $T \in \{5, 10, 15, 20, 25\}$ showing that the analytical results can be accurately reproduced.

5.2. Random matrix strength and constant bond

Semi-analytical model of stochastic cracking considering random matrix strength has been introduced by Curtin *et al.* [35]. Given a Weibull distribution of matrix strength with the scale parameter σ_R and shape parameter m they related the matrix strength distribution to the probability distribution of the crack spacing for a given level of load σ_c in form of a differential equation and initial conditions. By solving the resulting initial value problem, one could evaluate the crack spacing at the saturated state for given parameters of the random strength distribution. The comparison this model to PMCM is performed in terms of the relation between the shielded length and final crack spacing Λ, which has been derived analytically in [22] to yield the value 1.337 for the so-called car parking problem. This result can be expected for the composite fragmentation assuming constant matrix strength. The relation between the final crack spacing and the scatter of matrix strength expressed by Weibull modulus m is shown in terms of the dimensionless variable Λ in Fig. 9a. Apparently, in case of $m \to \infty$ (quasi constant matrix strength), Λ equals 1.337 and the model is equivalent to the ACK model. The average crack spacing of a composite with given volume fractions and bond properties is then obtained as

$$\ell_S = \Lambda(m) \frac{V_m \sigma_R}{V_f T}. \tag{27}$$

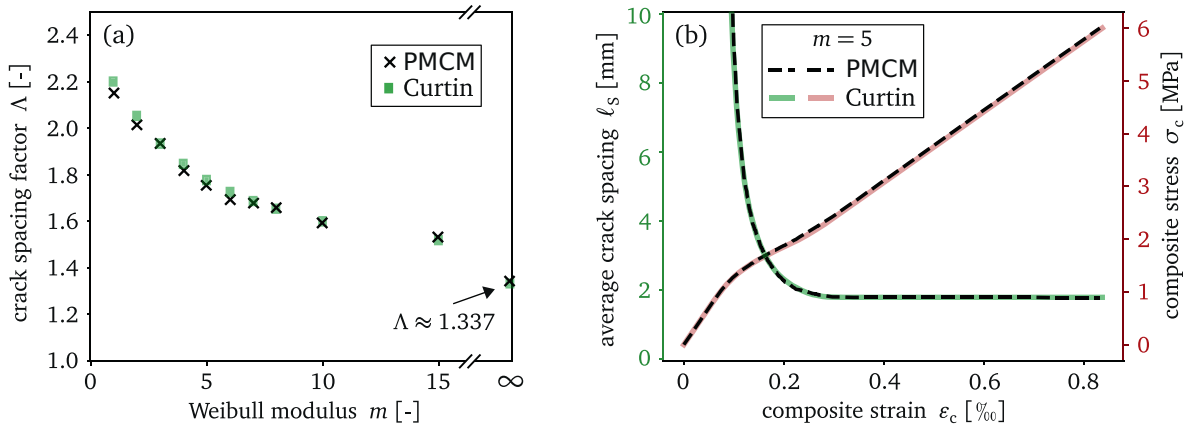

Fig. 9. Reproduction of the analytical solution in [55]: (a) Λ as a function of m; (b) the crack development and the stress-strain curve for $m = 5$.

Table 2
Parameters used in the PMCM.

parameter	notation	value	unit
bond intensity	T	9.0	N/mm^3
reinforcement ratio	V_f	10%	–
reinforcement modulus	E_f	67 000	MPa
matrix modulus	E_m	8 250	MPa
scale parameter	σ_R	1.0	MPa
reference length	L_R	2.0	mm
slice length	l_e	0.083	mm

With the final value of crack spacing at hand, the average crack spacing $\bar{\ell}$ at a stress level σ_c is related to the probability distribution of the matrix strength by the equality [54]

$$\frac{\bar{\ell}(\sigma_c)}{\ell_S} = 1 - \exp\left[-\left(\frac{\sigma_c}{\sigma_R}\right)^m\right]. \tag{28}$$

An example of evaluated average crack spacing evolution for $m = 5$ is shown in Fig. 9(b) as a green solid curve. Using the average crack spacing, the stress-strain curve shown as a pink solid curve in Fig. 9(b) can be obtained using the relation (see e.g. [23])

$$\varepsilon_c(\sigma_c) = \begin{cases} \dfrac{\sigma_c}{E_f V_f} - \dfrac{T\bar{\ell}(\sigma_c)}{4E_f}, & \bar{\ell}(\sigma_c) \le 2\delta_c(\sigma_c) \\ \dfrac{\sigma_c}{E_c}\left(1 + \dfrac{E_m V_m \delta_c(\sigma_c)}{E_f V_f \bar{\ell}(\sigma_c)}\right), & \bar{\ell}(\sigma_c) > 2\delta_c(\sigma_c) \end{cases} \tag{29}$$

where δ_c represents the stress recovery length defined as

$$\delta_c(\sigma_c) = \frac{V_m E_m \sigma_c}{V_f E_c T}. \tag{30}$$

To obtain a consistent discretization with the random matrix field used in PMCM, the scale parameter of the Weibull distribution has been adjusted for the length of the discretization element l_e using the scaling

$$\sigma_e = \sigma_R \left(\frac{l_e}{l_R}\right)^{-1/m}, \tag{31}$$

where L_R is the reference length for the Weibull distribution parameters σ_R and m. With the parameters summarized in Table 2, the value of Λ is evaluated for $m \in \{1, 2, 3, 4, 5, 6, 7, 8, 10, 15, 10000\}$ ($m = 10,000$ mimics the case of constant matrix strength), the results are depicted in Fig. 9(a) along with the analytical solution derived in [55]. The analytical and numerical values fit well with each other. To demonstrate the ability of the model to reproduce also the evolution of crack

Table 3
Relevant material parameters extracted from [23] .

parameter	notation	value	unit
bond intensity	T	126.4	N/mm^3
reinforcement ratio	V_f	10.4%	–
reinforcement modulus	E_f	72 000	MPa
matrix modulus	E_m	18 000	MPa
scale parameter	σ_R	14.8	MPa
Weibull modulus	m	1.4	–

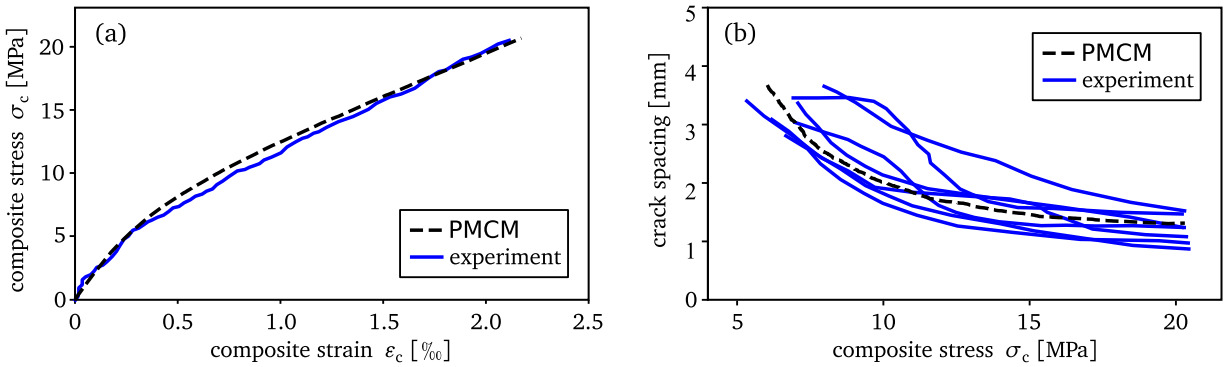

Fig. 10. Simulation of experimental results in [23]: (a) stress-strain curves; (b) crack development.

spacing and stress-strain relationship, these curves have been calculated for $m = 5$ and plotted in Fig. 9(b) as well. The results of the PMCM match exactly the analytical solution.

6. Application to cementitious composites

To demonstrate the applicability of PMCM to practical engineering composites, we use the model to numerically reproduce the experimental results reported in [23]. Specimens of inorganic phosphate cement reinforced by glass fiber fabrics were tested under uni-axial tensile loads. During the testing, the stress-strain relationships and the average crack spacing were recorded. All the relevant material parameters required by PMCM to reproduce these data were provided in [23] as summarized by Table 3. We directly use them as inputs for PMCM to simulate the experiments. The numerically reproduced results are plotted in Fig. 10 along with the experimental data.

As Fig. 10 shows, the simulation agrees well with the experiments in terms of both the stress-strain relationship and the crack spacing evolution. Since the parameters are directly taken from [23], we note that the purpose here is not to validate the model through a rigorous calibration-validation program, but to demonstrate that the model can correctly reproduce the tensile behavior of practical engineering materials. The calibration and validation method is described in [39] with crack bridge tests and uni-axial tensile tests on textile reinforced concrete.

7. Conclusions

The paper presents a general modeling framework for the uniaxial tensile behavior of brittle-matrix composites. A robust crack tracing algorithm is proposed to identify the multiple crack process. It is formulated in such a way that it can be combined with a variety of crack bridge models at the meso scale to consider different types of materials. The model can well capture the strain-hardening and multiple cracking behavior. To demonstrate the efficiency and robustness of the algorithm an interactive open-source web application has been provided in a github.com repository [46] that can be launched by following the launch link provided in the repository.

In combination with the simple crack bridge model considering a constant bond, the PMCM is verified against the analytical ACK model and the Curtin model. Good agreements between the PMCM and the analytical models have been observed, which demonstrate that the PMCM can capture the random cracking process in composite when a constant bond in bond interface is considered.

We also qualitatively demonstrated the difference between the proposed crack tracking algorithm and the existing models, it can properly handle the possible non-monotonic variations in the matrix stress introduced by complex bond interface behavior. This feature is important for the application presented in [39], where the PMCM is used in combination with the probabilistic crack model [50] to simulate tensile behavior of non-impregnated carbon textile reinforced concrete. A sys-

tematic calibration-validation procedure of the model parameters is presented in [39] to fully demonstrate the capability of PMCM.

Acknowledgements

The first and fourth authors acknowledge financial support provided by the Deutsche Forschungsgemeinschaft (DFG, German Research Foundation) - SFB/TRR280, Project-ID 417002380. The second author was supported by the China Postdoctoral Science Foundation (2019M662916). The last author acknowledges financial support provided by the Czech Science Foundation under project No. GC19-06684J.

Appendix A. Implementation

For the reader's convenience, the code is provided in a directly executable form in a public `github.com` repository [46] and can be started without local installation by following the launch link. The material parameters can be easily controlled in the provided range providing the result in terms of an immediately updated stress-strain curve and crack distribution along the tensile specimen.

The code can also be installed and executed within a standard `Python`-based computing environment that contains two standard numerical packages: `numpy` (line 1) providing efficient operators on multi-dimensional arrays and `scipy` (line 2) offering a broad infrastructure for scientific computing [56]. The whole bundle of the Python packages can be easily installed using the open-source distribution of `anaconda` suite (www.anaconda.com) on any current computer platform. To complete the picture, the core part of the code reflecting abstract description of the algorithm is printed and briefly explained here.

The crack bridge model with constant bond described by Eqs. (12) and (14) is implemented in the two functions on lines 14 and 18, respectively.

The tensile specimen of 500 mm length is discretized into a series of 5000 material elements (line 23) and the coordinates of the mid points of the material elements are stored in the array `x`. The spatial randomness in matrix strength (Eq. 2) is simply represented by a sequence of independent draws from the Weibull random variable a large shape parameter $m = 10000$ (corresponding to nearly zero scatter) on line 23. In this way the verification to the ACK model discussed in Section 5.1 can be performed.

The function `get_z_x` defined at line 26 implements the mapping between the global and local coordinates x and z given Eq. (15). It returns an array of distances between each material point and its closest crack.

The function `get_sig_c_z` delivers the load initiating a crack at a material point with the distance `z` from its closest crack, see Eq. (5). The `newton` method from the `scipy` [56] package is adopted to solve this nonlinear equation. It starts the search at the load level that initiated the previous crack, i.e., $\sigma^{(K-1)}$. When no solution can be found a `RuntimeWarning` is issued or a `RuntimeError` is raised. This indicates the current material point is within the shielded zone, and the function simply returns the composite strength to mark that no further crack can emerge at this position. To enable the possible `RuntimeWarning` handled by the `except` mechanism, it must be treated as an `Error` as done on lines 30 and 31. The function `get_sig_c_K` utilizes the function `get_sig_c_z` to evaluate the crack initiating loads in every material point of the specimen and to identify their minimum as the crack initiating load of the current step, see Eqs. (6) and (7).

The function `get_cracking_history` implements the loop identifying all cracks (see Fig. 4). In line 62, if the program find that the cracking load equals the composite strength, meaning that each material point is covered by the shielded zone, it determines all the cracks are found and the loop should end. In the present simple case, the average strains are directly computed in each step according to Eq. (14) by the line 67, no further post-processing is required.

Finally, the stress-strain shown in Fig. 8 is calculated and plotted on lines 73-75.

```
import numpy as np
from scipy.optimize import newton
import pylab as plt

Em = 25e3  # [MPa] matrix modulus
Ef = 180e3  # [MPa] fiber modulus
vf = 0.01  # reinforcement ratio
T = 12.  # bond intensity
Ec = Em * (1-vf) + Ef*vf # [MPa] mixture rule
sig_cu = 10.0 # [MPa] composite strength
sig_mu = 3.0 # [MPa] matrix strength
m = 10000 # Weibull shape modulus

def get_sig_m(z, sig_c):  # matrix stress
    sig_m = np.minimum(z * T * vf / (1 - vf), Em * sig_c / (vf * Ef + (1 - vf) * Em))
    return sig_m

def get_eps_f(z, sig_c):  # reinforcement strain
    sig_m = get_sig_m(z, sig_c)
    eps_f = (sig_c - sig_m * (1 - vf)) / vf / Ef
    return eps_f

x = np.linspace(0, 500, 5000)  # specimen discretization
sig_mu_x = 3.0 * np.random.weibull(m, size=5000) # matrix strength

def get_z_x(x, XK):  # distance to the closest crack
    z_grid = np.abs(x[:, np.newaxis] - np.array(XK)[np.newaxis, :])
    return np.amin(z_grid, axis=1)

import warnings
warnings.filterwarnings("error", category=RuntimeWarning)
def get_sig_c_z(sig_mu, z, sig_c_pre):
    # crack initiating load at a material element
    fun = lambda sig_c: sig_mu - get_sig_m(z, sig_c)
    try:  # search for the local crack load level
        return newton(fun, sig_c_pre)
    except (RuntimeWarning, RuntimeError):
        # solution not found (shielded zone) return the ultimate composite strength
        return sig_cu

def get_sig_c_K(z_x, sig_c_pre):
    # crack initiating loads over the whole specimen
    get_sig_c_x = np.vectorize(get_sig_c_z)
    sig_c_x = get_sig_c_x(sig_mu_x, z_x, sig_c_pre)
    y_idx = np.argmin(sig_c_x)
    return sig_c_x[y_idx], x[y_idx]

def get_cracking_history():
    XK = [] # recording the crack postions
    sig_c_K = [0.] # recording the crack initating loads
    eps_c_K = [0.] # recording the composite strains

    idx_0 = np.argmin(sig_mu_x)
    XK.append(x[idx_0])  # position of the first crack
    sig_c_0 = sig_mu_x[idx_0] * Ec / Em
    sig_c_K.append(sig_c_0)
    eps_c_K.append(sig_mu_x[idx_0] / Em)

    while True:
        z_x = get_z_x(x, XK)
        sig_c_k, y_i = get_sig_c_K(z_x, sig_c_K[-1])
        if sig_c_k == sig_cu:
            break
        XK.append(y_i)
        sig_c_K.append(sig_c_k)
        eps_c_K.append(
        np.trapz(get_eps_f(get_z_x(x, XK), sig_c_k), x) / np.amax(x))

    sig_c_K.append(sig_cu) # the ultimate state
    eps_c_K.append(np.trapz(get_eps_f(get_z_x(x, XK), sig_cu), x) / np.amax(x))
    return sig_c_K, eps_c_K

sig_c_K, eps_c_K = get_cracking_history()
plt.plot(eps_c_K, sig_c_K)
plt.show()
```

References

[1] R. Chudoba, E. Sharei, A. Scholzen, A strain-hardening microplane damage model for thin-walled textile-reinforced concrete shells, calibration procedure, and experimental validation, Composite Structures 152 (2016) 913–928, doi:10.1016/j.compstruct.2016.06.030.
[2] M.A.E.M. Ali, A.M. Soliman, M.L. Nehdi, Hybrid-fiber reinforced engineered cementitious composite under tensile and impact loading, Materials & Design 117 (2017) 139–149, doi:10.1016/j.matdes.2016.12.047.
[3] T. Gong, A.H. Ahmed, I. Curosu, V. Mechtcherine, Tensile behavior of hybrid fiber reinforced composites made of strain-hardening cement-based composites (SHCC) and carbon textile, Constr. Build. Mater. 262 (2020) 120913, doi:10.1016/j.conbuildmat.2020.120913.
[4] Z. Dong, M. Deng, C. Zhang, Y. Zhang, H. Sun, Tensile behavior of glass textile reinforced mortar (TRM) added with short PVA fibers, Constr. Build. Mater. 260 (2020) 119897, doi:10.1016/j.conbuildmat.2020.119897.
[5] P. Valeri, M. Fernández Ruiz, A. Muttoni, Tensile response of textile reinforced concrete, Constr. Build. Mater. 258 (2020) 119517, doi:10.1016/j.conbuildmat.2020.119517.
[6] B. Mobasher, A. Peled, J. Pahilajani, Distributed cracking and stiffness degradation in fabric-cement composites, Mater. Struct. 39 (3) (2006) 317–331, doi:10.1007/s11527-005-9005-8.
[7] J.D. Ríos, C. Leiva, M.P. Ariza, S. Seitl, H. Cifuentes, Analysis of the tensile fracture properties of ultra-high-strength fiber-reinforced concrete with different types of steel fibers by x-ray tomography, Materials & Design 165 (2019) 107582, doi:10.1016/j.matdes.2019.107582.
[8] C. Chen, H. Cai, J. Li, P. Zhong, B. Huang, L. Sui, Y. Zhou, One-Dimensional extended FEM based approach for predicting the tensile behavior of SHCC-FRP composites, Eng Fract Mech 225 (2020) 106775, doi:10.1016/j.engfracmech.2019.106775.
[9] Y. Goldfeld, Structural modelling of textile-reinforced concrete elements under uniaxial tensile loading, Compos Struct 235 (2020) 111805, doi:10.1016/j.compstruct.2019.111805.
[10] E. Grande, G. Milani, Numerical simulation of the tensile behavior of FRCM strengthening systems, Composites Part B: Engineering 189 (2020) 107886, doi:10.1016/j.compositesb.2020.107886.
[11] M.H. Al-Majidi, A. Lampropoulos, A.B. Cundy, Tensile properties of a novel fibre reinforced geopolymer composite with enhanced strain hardening characteristics, Composite Structures 168 (2017) 402–427, doi:10.1016/j.compstruct.2017.01.085.
[12] Y. Swolfs, Y. Meerten, P. Hine, I. Ward, I. Verpoest, L. Gorbatikh, Introducing ductility in hybrid carbon fibre/self-reinforced composites through control of the damage mechanisms, Composite Structures 131 (2015) 259–265, doi:10.1016/j.compstruct.2015.04.069.
[13] C. Wu, V.C. Li, CFRP-ECC hybrid for strengthening of the concrete structures, Composite Structures 178 (2017) 372–382, doi:10.1016/j.compstruct.2017.07.034.
[14] W. Brameshuber, M. Hinzen, A. Dubey, A. Peled, B. Mobasher, A. Bentur, C. Aldea, F. Silva, J. Hegger, T. Gries, Recommendation of RILEM TC 232-TDT: test methods and design of textile reinforced concrete: uniaxial tensile test: test method to determine the load bearing behavior of tensile specimens made of textile reinforced concrete, Mater. Struct. 49 (12) (2016) 4923–4927, doi:10.1617/s11527-016-0839-z.
[15] A. Scholzen, R. Chudoba, J. Hegger, Thin-walled shell structures made of textile-reinforced concrete: part II: experimental characterization, ultimate limit state assessment and numerical simulation, Structural Concrete 16 (1) (2015) 115–124, doi:10.1002/suco.201400046.
[16] D. Marshall, B. Cox, A. Evans, The mechanics of matrix cracking in brittle-matrix fiber composites, Acta Metall. 33 (11) (1985) 2013–2021, doi:10.1016/0001-6160(85)90124-5.
[17] W. Curtin, Multiple matrix cracking in brittle matrix composites, Acta metall. mater. 41 (5) (1993) 1369–1377, doi:10.1016/0956-7151(93)90246-O.
[18] Y. Li, J. Bielak, J. Hegger, R. Chudoba, An incremental inverse analysis procedure for identification of bond-slip laws in composites applied to textile reinforced concrete, Composites Part B: Engineering 137 (2018) 111–122, doi:10.1016/j.compositesb.2017.11.014.
[19] J. Aveston, G. Cooper, A. Kelly, Single and multiple fracture: The properties of fibre composites, in: Proc. Conf. National Physical Laboratories, IPC Science and Technology Press Ltd. London, 1971, pp. 15–24.
[20] A. Kimber, J. Keer, On the theoretical average crack spacing in brittle matrix composites containing continuous aligned fibres, J Mater Sci Lett 1 (8) (1982) 353–354, doi:10.1007/BF00726486.
[21] A. Rényi, On a one-dimensional problem concerning space filling, Magyar Tud. Akad. Matematikai Kut. Intez. Kozl. 3 (1958) 109–127.
[22] B. Widom, Random sequential addition of hard spheres to a volume, J Chem Phys 44 (1966) 3888–3894, doi:10.1063/1.1726548.
[23] H. Cuypers, J. Wastiels, Stochastic matrix-cracking model for textile reinforced cementitious composites under tensile loading, Mater. Struct. 39 (8) (2006) 777–786, doi:10.1617/s11527-005-9053-0.
[24] J. Aveston, A. Kelly, Theory of multiple fracture of fibrous composites, J Mater Sci 8 (3) (1973) 352–362, doi:10.1007/BF00550155.
[25] B. Budiansky, J. Hutchinson, A. Evans, Matrix fracture in fiber-reinforced ceramics, J Mech Phys Solids 34 (2) (1986) 167–189, doi:10.1016/0022-5096(86)90035-9.
[26] C. Cho, J. Holmes, J. Barber, Distribution of matrix cracks in a uniaxial ceramic composite, J. Am. Ceram. Soc. 2 (75) (1992) 316–324, doi:10.1111/j.1151-2916.1992.tb08181.x.
[27] C.-Y. Hui, S. Phoenix, M. Ibnabdeljalil, R. Smith, An exact closed form solution for fragmentation of Weibull fibers in a single filament composite with applications to fiber-reinforced ceramics, J Mech Phys Solids 43 (10) (1995) 1551–1585, doi:10.1016/0022-5096(95)00045-K.
[28] E. Castelier, L. Gélébart, C. Lacour, C. Lantuéjoul, Three consistent approaches of the multiple cracking process in 1D composites, Compos Sci Technol 70 (15) (2010) 2146–2153, doi:10.1016/j.compscitech.2010.08.014.
[29] W. Curtin, The tough to brittle transition in brittle matrix composites, J Mech Phys Solids 41 (2) (1993) 217–245, doi:10.1016/0022-5096(93)90007-3.
[30] D. Harlow, S. Phoenix, The chain-of-bundles probability model for the strength of fibrous materials I: analysis and conjectures, J Compos Mater 12 (2) (1978) 195–214, doi:10.1177/002199837801200207.
[31] D. Harlow, S. Phoenix, The chain-of-bundles probability model for the strength of fibrous materials II: a numerical study of convergence, J Compos Mater 12 (3) (1978) 314–334, doi:10.1177/002199837801200308.
[32] J. Kang, J.E. Bolander, Multiscale modeling of strain-hardening cementitious composites, Mech Res Commun 78, Part B (2016) 47–54, doi:10.1016/j.mechrescom.2015.08.004.
[33] A. Netravali, R. Henstenburg, S. Phoenix, P. Schwartz, Interfacial shear strength studies using the single-filament-composite test. i: experiments on graphite fibers in epoxy, Polym Compos 10 (4) (1989) 226–241, doi:10.1002/pc.750100405.
[34] R. Henstenburg, S. Phoenix, Interfacial shear strength studies using the single-filament-composite test. Part II: a probability model and Monte Carlo simulation, Polym Compos 10 (5) (1989) 389–408, doi:10.1002/pc.750100603.
[35] W. Curtin, Exact theory of fiber fragmentation in a single-filament composite, J Mater Sci 26 (1991) 5239–5253, doi:10.1007/BF01143218.
[36] S. Zhang, X. Gao, Y. Song, In situ strength model for continuous fibers and multi-scale modeling the fracture of C/SiC composites, Appl Compos Mater 26 (2019) 357–370, doi:10.1007/s10443-018-9696-y.
[37] R. Santoro, G. Failla, G. Muscolino, Interval static analysis of multi-cracked beams with uncertain size and position of cracks, Applied Mathematical Modelling 86 (2020) 92–114, doi:10.1016/j.apm.2020.03.049.
[38] S.-P. Zhu, Y.-Z. Hao, D. Liao, Probabilistic modeling and simulation of multiple surface crack propagation and coalescence, Applied Mathematical Modelling 78 (2020) 383–398, doi:10.1016/j.apm.2019.09.045.
[39] M. Vořechovský, R. Chudoba, Y. Li, R. Rypl, Probabilistic multiple cracking model of elastic-brittle matrix composite reflecting randomness in matrix, reinforcement and bond, in: Computational Modelling of Concrete Structures, CRC Press, Bad Hofgastein, 2018, pp. 839–848, doi:10.1201/9781315182964.
[40] Y. Li, R. Chudoba, J. Bielak, J. Hegger, A Modelling Framework for the Tensile Behavior of Multiple Cracking Composite, in: International Conference on Strain-Hardening Cement-Based Composites, Springer, 2017, pp. 418–426, doi:10.1007/978-94-024-1194-2_49.
[41] R. Rypl, R. Chudoba, A. Scholzen, M. Vořechovský, Brittle matrix composites with heterogeneous reinforcement: multi-scale model of a crack bridge with rigid matrix, Compos Sci Technol 89 (2013) 98–109, doi:10.1016/j.compscitech.2013.09.014.

[42] G. Hernandez, R. Leon, L. Salinas, E. Dimnet, A fragmentation model with neighborhood interaction, Applied Mathematical Modelling 36 (4) (2012) 1694–1702, doi:10.1016/j.apm.2011.09.019.
[43] A. Dedner, B. Kane, R. Klöfkorn, M. Nolte, Python framework for hp-adaptive discontinuous Galerkin methods for two-phase flow in porous media, Applied Mathematical Modelling 67 (2019) 179–200, doi:10.1016/j.apm.2018.10.013.
[44] C. Lu, C.K. Leung, V.C. Li, Numerical model on the stress field and multiple cracking behavior of engineered cementitious composites (ECC), Construction and Building Materials 133 (Supplement C) (2017) 118–127, doi:10.1016/j.conbuildmat.2016.12.033.
[45] R. Chudoba, V. Sadílek, R. Rypl, M. Vořechovský, Using python for scientific computing: efficient and flexible evaluation of the statistical characteristics of functions with multivariate random inputs, Comput Phys Commun 184 (2) (2013) 414–427, doi:10.1016/j.cpc.2012.08.021.
[46] R. Chudoba, Y. Li, R. Rypl, H. Spartali, M. Vořechovský, bmcs-group/bmcs_fragmentation: Paper-Submission release (2020), doi:10.5281/zenodo.3886956.
[47] Z. Lin, V.C. Li, Crack bridging in fiber reinforced cementitious composites with slip-hardening interfaces, J Mech Phys Solids 45 (5) (1997) 763–787, doi:10.1016/S0022-5096(96)00095-6.
[48] T. Huang, Y. Zhang, C. Su, S. Lo, Effect of slip-hardening interface behavior on fiber rupture and crack bridging in fiber-reinforced cementitious composites, J. Eng. Mech. 141 (10) (2015) 04015035, doi:10.1061/(ASCE)EM.1943-7889.0000932.
[49] Y. Li, R. Chudoba, J. Bielak, J. Hegger, A modelling framework for the tensile behavior of multiple cracking composite, in: V. Mechtcherine, V. Slowik, P. Kabele (Eds.), Strain-Hardening Cement-Based Composites (SHCC 2017), RILEM Bookseries, 15, Springer, 2018, pp. 418–426, doi:10.1007/978-94-024-1194-2_49.
[50] M. Vořechovský, R. Rypl, R. Chudoba, Probabilistic crack bridge model reflecting random bond properties and elastic matrix deformation, Composites Part B: Engineering 139 (2018) 130–145, doi:10.1016/j.compositesb.2017.11.040.
[51] A.T. DiBenedetto, M.R. Gurvich, Statistical simulation of fiber fragmentation in a single-fiber composite, Compos Sci Technol 57 (5) (1997) 543–555, doi:10.1016/S0266-3538(97)00008-0.
[52] W. Curtin, B. Ahn, N. Takeda, Modeling brittle and tough stress-strain behavior in unidirectional ceramic matrix composites, Acta Mater 46 (10) (1998) 3409–3420, doi:10.1016/S1359-6454(98)00041-X.
[53] P. Larrinaga, C. Chastre, J. San-José, L. Garmendia, Non-linear analytical model of composites based on basalt textile reinforced mortar under uniaxial tension, Composites Part B: Engineering 55 (2013) 518–527, doi:10.1016/j.compositesb.2013.06.043.
[54] B. Ahn, W. Curtin, Strain and hysteresis by stochastic matrix cracking in ceramic matrix composites, J Mech Phys Solids 45 (2) (1997) 177–209, doi:10.1016/S0022-5096(96)00081-6.
[55] W. Curtin, Stochastic damage evolution and failure in fiber-reinforced composites, Advances in Applied Mechanics, Vol 36 36 (1999) 163–253, doi:10.1016/S0065-2156(08)70186-8.
[56] P. Virtanen, R. Gommers, T.E. Oliphant, M. Haberland, T. Reddy, D. Cournapeau, E. Burovski, P. Peterson, W. Weckesser, J. Bright, S.J. van der Walt, M. Brett, J. Wilson, K. Jarrod Millman, N. Mayorov, A.R.J. Nelson, E. Jones, R. Kern, E. Larson, C. Carey, İ. Polat, Y. Feng, E.W. Moore, J. Vand erPlas, D. Laxalde, J. Perktold, R. Cimrman, I. Henriksen, E.A. Quintero, C.R. Harris, A.M. Archibald, A.H. Ribeiro, F. Pedregosa, P. van Mulbregt, S.. Contributors, SciPy 1.0: fundamental algorithms for scientific computing in python, Nat. Methods 17 (2020) 261–272, doi:10.1038/s41592-019-0686-2.

View publication stats